MATERIALS CHEMISTRY
FRONTIERS

RESEARCH ARTICLE

View Article Online
View Journal | View Issue

Cite this: *Mater. Chem. Front.*, 2021, **5**, 4690

Synthesis and fundamental studies of a photoresponsive oligonucleotide-upconverting nanoparticle covalent conjugate†

Christopher Liczner, [a] Gabrielle A. Mandl, [ab] Steven L. Maurizio, [ab] Kieran Duke,[a] John A. Capobianco *[ab] and Christopher J. Wilds *[a]

Received 25th March 2021,
Accepted 24th April 2021

DOI: 10.1039/d1qm00467k

rsc.li/frontiers-materials

Photo-mediated systems present a highly attractive route for controlling the intracellular delivery of their cargo. Of particular interest, oligonucleotides are a promising class of molecule that are highly versatile for intracellular applications, but lack the necessary *in vivo* stability on their own. A novel, greener synthetic route to a photocleavable phosphoramidite was developed. The amidite was incorporated into an oligonucleotide by solid-phase synthesis, which was covalently linked to UV-emissive lanthanide-doped upconverting nanoparticles (UCNPs) through click chemistry. The nanosystem was fully characterized for energy transfer dynamics between the photocleavable oligonucleotide and UCNP using 976 nm excitation. The practical and green synthesis of the photocleavable phosphoramidite, combined with the fundamental understanding of the interactions between the oligonucleotide and nanoparticle during excitation paves the way for future *in vitro* applications for this type of system.

Introduction

Synthetic oligonucleotides have shown great utility in the fields of diagnostics (biosensing[1–3]) and therapeutics (gene silencing by antisense[4] or RNA interference[5] mechanisms). Some of the challenges in employing oligonucleotides for these applications, however, include their susceptibility to nuclease degradation in serum, poor cellular uptake, as well as unfavorable bio-distribution and targeting. The current strategies employed to improve the properties of oligonucleotides for intracellular delivery are the chemical modification of the sugar-phosphate backbone[6–8] and/or conjugation to smaller ligands (*e.g.*: *N*-acetylgalactosamine–GalNAc,[9] peptides[10]) or nanoparticles (*e.g.*: polymers,[11] gold,[12] lipids[13]). Nanoparticle–oligonucleotide conjugates represent one of the most well-studied platforms and have shown to improve cellular uptake, circulation time and endosomal escape of oligonucleotides, while also further protecting them from nucleolytic degradation.[14]

A highly attractive route for the delivery of oligonucleotides employs lanthanide-doped upconverting nanoparticles (UNCPs) with *in situ* photo-mediated release of the nucleic acid payload. Upconversion is an anti-Stokes luminescence phenomenon in which the successive absorption of low-energy photons results in the promotion of electrons to the long-lived excited 4f states of lanthanide ions and subsequent radiative relaxation results in the production of higher-energy emissions in the UV, visible and near infrared (NIR). Importantly, the emitted UV light from UCNPs has been shown to not be damaging to living organisms.[15] It is well-established that energy transfer upconversion, which utilizes a NIR-absorbing sensitizer ion (commonly Yb^{3+} or Nd^{3+}) and an emissive activator ion, is the most efficient mechanism. Fluoride-based UCNPs exhibit excellent chemical stability, do not photobleach or photoblink, have low-phonon energies and thus far, exhibit minimal cytotoxicity.[16] For these reasons, fluoride-based UCNPs have found wide use for biomedical applications such as imaging and drug delivery. With regard to host compositions, $LiYF_4$ is a commonly overlooked material that facilitates strong upconversion in the UV when doped with 25 mol% Yb^{3+} and 0.2 mol% Tm^{3+}.[17] The upconverted emissions at 345 and 360 nm from the $^1I_6 \rightarrow {}^3F_4$ and $^1D_2 \rightarrow {}^3H_6$ transitions of Tm^{3+} have been used for a wide variety of photochemistry applications that require *in situ* UV activation.[18,19] Of particular interest, the UV emissions from Tm^{3+} exhibit excellent spectral overlap with the photocleavable *o*-nitrobenzyl linker, which is well-known for its photocaging applications.[20] Oligonucleotide-functionalized UCNPs have been recognized for their potential for intracellular sensing and imaging applications,[3,21] as UCNP emissions can be achieved through NIR excitation, avoiding deleterious signals

[a] *Department of Chemistry and Biochemistry, Concordia University, 7141 Rue Sherbrooke Ouest, Montréal, QC, H4B 1R6, Canada. E-mail: chris.wilds@concordia.ca*
[b] *Centre for NanoScience Research, Concordia University, 7141 Rue Sherbrooke Ouest, Montréal, QC, H4B 1R6, Canada. E-mail: john.capobianco@concordia.ca*

† Electronic supplementary information (ESI) available. See DOI: 10.1039/d1qm00467k

from autofluorescence in tissues.[22] Photomediated release of therapeutic oligonucleotides, however, has only been demonstrated on a few occasions.[23,24] Complex formation between the surface-modified UCNPs and oligonucleotides is typically the result of electrostatic interactions. One such example, reported in 2013, was a UCNP–oligonucleotide conjugate for intracellular delivery of short interfering RNA (siRNA) that showed *in vitro* knockdown of an enhanced green fluorescent protein (eGFP) gene.[23] In this system, $NaYF_4$ doped with Tm^{3+} and Yb^{3+} UCNPs were silica-coated and functionalized with a cationic and photocleavable *o*-nitrobenzyl linker through a thiosuccinimide linkage (Fig. 1A). With the siRNA electrostatically bound to the UCNPs, the particles were shown to efficiently enter HeLa cells and cause the loss of eGFP fluorescence only upon irradiation with NIR light. This level of spatial and temporal control is quite attractive for *in vivo* drug delivery. Since not all genes are ubiquitously expressed in every tissue, selective oligonucleotide release can potentially minimize off-target effects. Furthermore, NIR radiation is well suited for biological applications, as it displays high tissue penetration and low cytotoxicity.[25,26]

Thus, although the previous system successfully demonstrated *in vitro* gene knockdown as well as the effectiveness of such a platform, it suffers from some clear limitations. Multiple reports have demonstrated the instability of thiosuccinimide linkages under physiological conditions or in the presence of free thiols (*e.g.*: albumin, cysteine or glutathione in plasma), which are susceptible to a retro-Michael reaction or thiol exchange.[27–30] The use of such a linkage is expected to undergo some degree of pre-mature drug release before reaching its target.[31] Furthermore, while the utilization of cationic, photoresponsive moieties on the UCNP surface does facilitate a strong electrostatic interaction with the anionic phosphodiester backbone of the oligonucleotides, it is well-known that electrostatic interactions can be easily disrupted by the formation of a protein corona and interactions with other intracellular species.[32] Lastly, there is also a lack of compatibility for loading neutral species onto the UCNPs, of which there exists many non-ionic classes of modified oligonucleotides, such as methylphosphonate oligonucleotides,[33] amide backbone oligonucleotides[34] and phosphorodiamidate morpholinos (PMOs).[35] In fact, there are currently two PMO antisense drugs, Eteplirsen and Golodirsen, which are FDA approved for the treatment of Duchenne muscular dystrophy, and others currently being extensively developed.[36] PMO drugs are known to suffer from efficient renal clearance[37] owing to their minimal interaction with plasma proteins, and therefore, are expected to greatly benefit from nanoparticle formulations to increase circulation time and cellular uptake. Consequently, the use of covalent conjugation between UCNPs and oligonucleotides using copper-catalyzed azide–alkyne cycloaddition (CuAAC) click chemistry represents an attractive path towards highly controlled release of a variety of ionic or non-ionic oligonucleotides. While this strategy was previously used to form DNA–UCNP covalent conjugates for nanosensing and imaging applications,[21] it has not been explored as an approach for controlling the release of oligonucleotides.

Herein, we have developed a robust, versatile and expandable UCNP-based intracellular delivery platform for oligonucleotides (Fig. 1B) and quantified the loading of oligonucleotide and photocleavage efficiency utilizing a trityl assay. The greener synthesis of an alkyne and photocleavable phosphoramidite

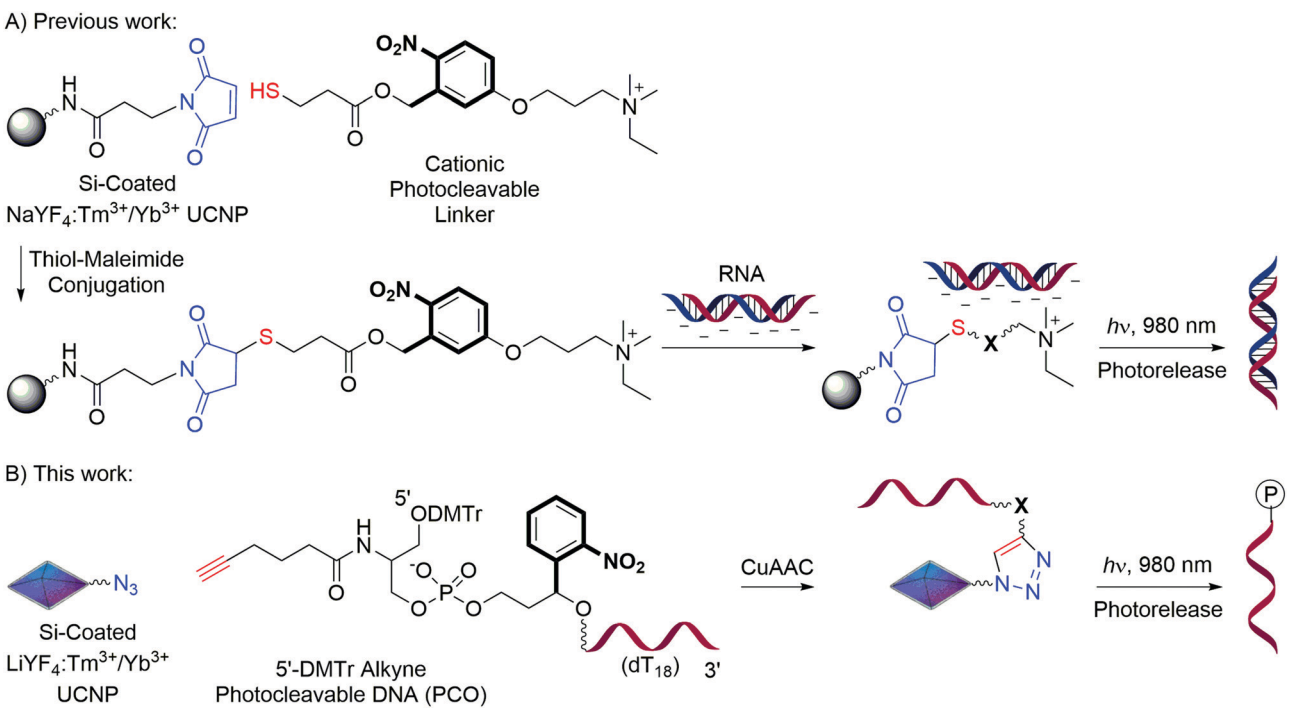

Fig. 1 Comparison of UCNP–oligonucleotide photorelease platforms (only 1 linker shown for clarity; X = *o*-nitrobenzyl group in bold; DMTr = dimethoxytrityl; P = phosphate).

(PCP) was achieved, which were subsequently incorporated at the 5′-end of an 18-mer homothymidine (dT_{18}) oligonucleotide by solid-phase synthesis (SPS). CuAAC click chemistry[38,39] was successfully utilized to generate a more robust triazole covalent linkage between the azide-functionalized silica-coated UCNPs (AzSiUCNPs) and alkyne photocleavable oligonucleotide (PCO). The system's efficient photorelease upon NIR irradiation was demonstrated and its luminescence dynamics was evaluated.

Results and discussion

Synthesis of alkyne and photocleavable phosphoramidites

A novel methodology for the synthesis of PCP **4** (which introduces the *o*-nitrobenzyl group into the oligonucleotide) was developed (Scheme 1). While this study does not solely focus on green chemistry, the importance of shifting synthetic strategies towards more sustainable practices[40] cannot be understated. By emphasizing the development of sustainable synthetic routes in academia, this could facilitate their translation to applicable industrial processes. To this end, the synthesis of the PCP was conceived with green aspects in mind, specifically atom economy, waste reduction and the inherent safety of the process. Commercially available 2-nitrobenzaldehyde was treated with vinylmagnesium bromide to afford allylic alcohol **1** with a yield of 70% (estimated by NMR) after acidic workup. The reaction could not be performed at 0 °C, as this resulted in the formation of unidentified side products and a drastic decrease in yield. Moreover, a 3 hour reaction time at −78 °C was necessary for full conversion of the 2-nitrobenzaldehyde, although any remaining starting material did not interfere with the subsequent reaction. Without purification, the hydroxyl group of allylic alcohol **1** was blocked by treatment with trimethylsilyl (TMS) chloride. Once complete, excess TMS-chloride was quenched with methanol and the solution concentrated *in vacuo*. The blocked intermediate was washed with tetrahydrofuran (THF) and filtered to remove the triethylamine (TEA) salt (observed to cause quenching of borane in the next step) and immediately treated with borane-THF. After oxidation, diol **2** was isolated with a yield of 74%. Selective tritylation of the primary alcohol, giving pre-amidite **3** with an isolated yield of 85% (no workup needed), followed by phosphitylation of the secondary alcohol afforded PCP **4** with an isolated yield of 83%. It should be noted, that TMS is not a protecting group in this synthesis, but rather a transient blocking group that affects the regioselectivity of hydroboration and is subsequently removed in the regular workflow by sodium hydroxide treatment during oxidation of the alkyl borane intermediate. Without TMS, hydroboration-oxidation gave 67% primary alcohol and 33% secondary alcohol, whereas when it was utilized, the proportion of the desired primary alcohol increased to 84%, as determined by NMR (see Fig. S14 and S15, ESI†) and thus, increased the isolated yield. The inductive effect of the allylic hydroxyl group is likely the main contributor for the poor regioselectivity observed,[41] which is minimized when sterically blocking the position. A bulkier group, such as *t*-butyldimethylsilyl, was not utilized in order to further improve regioselectivity as this silyl functionality is reported to be much more stable towards removal under basic conditions,[42] which would significantly increase the reaction time beyond the regular workflow. Additionally, while 9-borabicyclo[3.3.1]nonane is known to have enhanced anti-Markovnikov regioselectivity compared to borane,[43] the atom economy of the transformation is inferior and, for this hydroboration in particular, the 1,5-cyclooctanediol byproduct generated during oxidation made purification of the product diol cumbersome, lowering the isolated yield significantly.

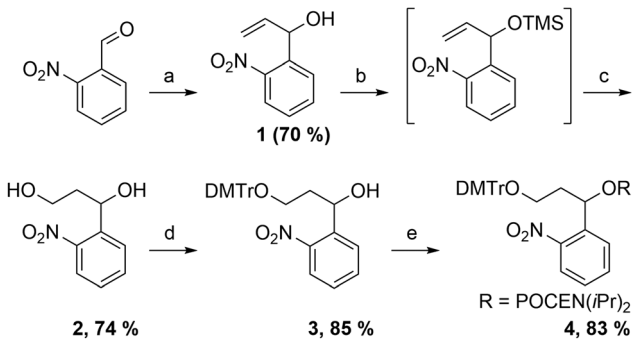

Scheme 1 Synthesis of photocleavable phosphoramidite **4**. *Reagents and conditions*: (a) vinylmagnesium bromide (2.0 equiv.), THF, −78 °C, 3 h; (b) TMS-Cl (3.0 equiv.), TEA (3.0 equiv.), DCM, 0 °C to RT, 1 h; (c) (i) BH_3-THF (4.0 equiv.), THF, 0 °C to RT, 19 h; (ii) 30% H_2O_2, 3 M NaOH, 0 °C to RT, 1 h; (d) DMTr-Cl (1.3 equiv.), TEA (2.6 equiv.), DMAP (10 mol%), DCM, 0 °C to RT, 1 h; (e) Cl-POCEN(iPr)$_2$ (2.0 equiv.), DIPEA (3.0 equiv.), DCM, RT, 25 min. (DCM = dichloromethane; DMAP = 4-dimethylaminopyridine; DIPEA = *N*,*N*-diisopropylethylamine.)

When compared to the previous route towards the PCP,[44] this synthesis provides some advantages. For example, ozonolysis, a hazardous reaction that generates potentially explosive ozonides, was avoided. Furthermore, the amount of solvent waste was significantly reduced, as it was not necessary to purify allylic alcohol **1** by flash column chromatography (FCC). Lastly, using stoichiometric amounts of vinylmagnesium bromide was more atom efficient than the previously employed Hosomi–Sakurai reaction that used stoichiometric allyltrimethylsilane and titanium tetrachloride (atom economy: 43% *vs.* 19%, respectively). While the second step uses TMS-Cl and TEA, where none of these atoms get incorporated into diol **2**, this is still superior to ozonolysis in the previous synthesis, which bubbled a large excess of ozone through the solution over 45 minutes. Not only was the synthesis of PCP **4** achieved in a greener fashion, it was also done more cost effectively (in terms of reagents), without the need for specialized equipment (ozone generator) and with a comparable overall yield of 37% over 4 steps (*vs.* 36% over 4 steps reported previously). Thus, the synthesis is not just environmentally more sustainable, but also more practical than the previous route.

Next, the synthesis of alkyne phosphoramidite **7** was undertaken (Scheme 2). This species, once incorporated into the oligonucleotide, would serve as the anchoring point between it and the UCNP, as well as provide the DMTr group for accurate loading quantification. The carboxylic acid starting material was first treated with isobutyl chloroformate (iBuOCOCl) and *N*-methylmorpholine (NMM) to generate the mixed anhydride

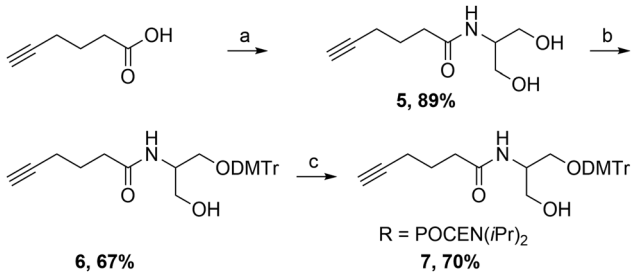

Scheme 2 Synthesis of alkyne phosphoramidite **7**. *Reagents and conditions*: (a) (i) iBuOCOCl (1.2 equiv.), NMM (2.4 equiv.), EtOAc, 0 °C, 40 min; (ii) serinol (1.0 equiv.), 0 °C to RT, 21 h; (b) DMTr-Cl (1.0 equiv.), TEA (2.0 equiv.), DMAP (10 mol%), THF, 0 °C to RT, 2.5 h; (c) Cl-POCEN(iPr)$_2$ (2.6 equiv.), DIPEA (2.9 equiv.), THF, RT, 30 min. (EtOAc = ethyl acetate; DMAP = 4-dimethylaminopyridine; DIPEA = *N*,*N*-diisopropylethylamine.)

intermediate. To this mixture was added serinol, affording amide **5** with an isolated yield of 89%. Treatment of amide **5** with dimethoxytrityl (DMTr) chloride afforded monotritylated pre-amidite **6** with 67% isolated yield. Even with slow, portion wise addition on ice of DMTr-chloride, generation of the ditritylated product was unavoidable. Finally, alkyne phosphoramidite **7** was isolated in 70% yield, generated by phosphitylating the remaining hydroxyl group.

Keeping greener synthetic approaches in mind, the use of heavy amide coupling reagents such as benzotriazol-1-yloxytripyrrolidinophosphonium hexafluorophosphate (PyBOP) or 2-(1*H*-benzotriazol-1-yl)-1,1,3,3-tetramethyluronium hexafluorophosphate (HBTU), was avoided, in favor of chloroformate. Thus, the atom economy of the amidation was maximized.

Synthesis and purification of 5′-O-DMTr alkyne photocleavable oligonucleotide (PCO) and control

The length of therapeutically relevant oligonucleotide drugs range from 18–30 nucleotides,[36] so, an 18-mer alkyne photocleavable oligonucleotide was conceived for this study. PCP **4** and alkyne phosphoramidites **7** were coupled, in that order, to the 5′-end of a dT$_{18}$ oligonucleotide by SPS (2 μmol scale) and the 5′-O-DMTr group was retained (shown in Fig. 1B). While it is agreed that protecting groups are generally not in line with atom economy, the SPS of oligonucleotides necessitates them due to the directionality of chain growth and the many reactive groups in the backbone and nucleobases, thus, they cannot be avoided altogether. Fortunately, some functionalities, such as DMTr, serve more than just their protective purpose in SPS. The DMTr group is used to quantify phosphoramidite coupling efficiency and loading of oligonucleotide (μmol of oligonucleotide per gram of solid-support), as well as aiding in the purification from inevitable failure sequences by either reversed-phase or ion-exchange (IEX) HPLC. Consequently, the DMTr group was an ideal candidate, previously unexplored, for quantifying the amount of oligonucleotide present on the surface of the AzSiUCNPs and subsequently, the photorelease efficiency upon NIR irradiation could be determined.

Before the PCO was cleaved from the solid-support, it was treated with 10% diethylamine in acetonitrile for 5 minutes in order to prevent the formation of acrylonitrile adducts at N3 of the thymine bases in the oligonucleotide during the deprotection step. Treatment with a solution of ammonium hydroxide/ethanol (3 : 1, v/v) at elevated temperatures subsequently released the oligonucleotide from the solid-support and deprotected the phosphodiester backbone. It was then determined that before lyophilization to dryness, it was imperative to add excess Tris (a non-volatile base) to the oligonucleotide solution in order to retain the DMTr group. As observed in the IEX HPLC traces, significant detritylation was observed if the PCO was lyophilized without Tris (Fig. S1, ESI†). These traces also demonstrate the usefulness of DMTr-on HPLC purification, as the desired tritylated oligonucleotides elute approximately 2–3 minutes after the detritylated or failure sequences, facilitating their isolation. The addition of Tris to retain the 5′-*O*-DMTr group throughout the entire oligonucleotide purification process could be instructive for the preparation of modified oligonucleotides. Furthermore, if detritylation is desired at a later stage of oligonucleotide purification, then this also represents ultra-mild, reagent-less conditions for detritylation (which can be achieved fully after just 2 successive lyophilizations). For example, this may be especially suitable for oligonucleotides containing 5′-end trityl-protected amines as it is preferential to remove the trityl group after cleavage from the solid-support and initial deprotection in order to avoid transamidation and cyanoethyl adduct formation at the free amine (although the latter case can be avoided by pre-treating the solid-support with diethylamine, as previously discussed).

The PCO was then purified by IEX HPLC to give approximately 6.6 mg (156 OD$_{260}$) of product with a purity of 97% (Fig. S2, ESI†) and confirmed to be the desired species by mass spectrometry (Fig. S3, ESI†). The 3% impurity was determined to be the DMTr-on alkyne photocleavable dT$_{17}$ sequence (Fig. S3, ESI†), and as such, was not deemed detrimental to the following studies. Importantly, keeping the DMTr-on PCO sample in 18 MΩ water at −20 °C for 3 months and re-analyzing by IEX HPLC demonstrated these conditions were adequate for long-term storage, as no additional detritylated oligonucleotide was observed in the trace (data not shown).

In order to illustrate the necessity of the *o*-nitrobenzyl functionality in the oligonucleotide to achieve proper photorelease, a non-photocleavable alkyne oligonucleotide was also synthesized. A control alkyne phosphoramidite (synthesized by phosphitylating 5-hexyn-1-ol; see ESI† for details) was coupled to the 5′-end of a dT$_{18}$ oligonucleotide by SPS (2 μmol scale). This sequence was isolated and purified as described for the PCO, but without the need for adding Tris prior to lyophilization as there was no 5′-*O*-DMTr (recovered approximately 6.5 mg; 170 OD$_{260}$). By IEX HPLC, the purity of the control sequence was determined to be 97% (Fig. S4, ESI†) and its identity confirmed by mass spectrometry (Fig. S5, ESI†).

Upconversion emission and physical characterization of UCNPs

LiYF$_4$:Yb^{3+}/Tm^{3+} UCNPs were synthesized *via* a one-pot thermal decomposition method to yield oleate-capped nanoparticles.[17] The nanoparticles exhibit a square bipyramidal morphology with an average size of 94 ± 6.2 nm along the long axis, and a

tetragonal crystal phase (Fig. 2A–C). The activator concentration of 0.2 mol% Tm^{3+} was chosen because it has been demonstrated to yield strong UV emissions in the $LiYF_4$ host,[17] which is necessary for obtaining efficient energy transfer with the *o*-nitrobenzyl group in the oligonucleotide backbone. An azide-functionalized silica shell was grafted onto the surface of the UCNPs *via* a reverse-microemulsion method to impart stability in aqueous environments as well as provide a platform for click chemistry to the alkyne-functionalized oligonucleotides. The average shell thickness was 11 nm along the edges, and 2 nm on the apices of each nanoparticle (Fig. 2B). The presence of the azide functional group was confirmed by FTIR (Fig. S6, ESI†) and a triphenylphosphine-ninhydrin assay, which exhibits a yellow colour in the presence of azides (Fig. S7, ESI†). Upconversion emission spectroscopy of the AzSiUCNPs dispersed in water (1 mg mL^{-1}) upon excitation at 976 nm exhibited the expected UV and blue emissions from Tm^{3+} at 288, 345, 360, 450 and 475 nm corresponding to the $^1I_6 \rightarrow {}^3H_6$, $^1I_6 \rightarrow {}^3F_4$, $^1D_2 \rightarrow {}^3H_6$, $^1D_2 \rightarrow {}^3F_4$ and $^1G_4 \rightarrow {}^3H_6$ transitions, respectively (Fig. 3A).

Quantification of azides and PCO on the surface of the UCNPs

Quantification of the number of azide sites generated on the nanoparticle surface was first carried out to determine the potential loading capacity of the nanoparticles using a DMTr assay. First, a 3′-*O*-propargyl thymidine (dT) nucleoside with a 5′-*O*-DMTr group (synthesized in one step from 5′-*O*-DMTr-dT; see ESI† for details) was grafted to the nanoparticle surface using CuAAC click chemistry. Because the nucleoside is small relative to the oligonucleotides, it was assumed that steric hindrance would not be a significant concern and that the click reaction would go to completion. This was confirmed qualitatively using the same triphenylphosphine-ninhydrin assay, which no longer showed a colour change (Fig. S7, ESI†). The dried nanoparticle samples were then dispersed in a solution of 3% trichloroacetic acid in dichloromethane (DCM), which resulted in the formation and release of the orange DMTr cation into solution. This DMTr cation has a strong absorption coefficient (76 L cm^{-1} mol^{-1} in DCM[45]) at 504 nm, which can be utilized to quantify the amount of DMTr in solution. Since each nucleoside contained one DMTr group, it can be concluded that the number of DMTr cations released into solution corresponded to the number of nucleosides clicked to the nanoparticle surface, and thus the number of azide groups. Using this method, it was determined that there was an average of 1.3×10^4 azide groups per nanoparticle (approximately 65 μmol g^{-1}). This is similar to the loadings exhibited on traditional controlled pore glass solid-supports for the SPS of oligonucleotides, which typically range from 30–100 μmol g^{-1}.[46] It is also comparable to the number of cationic photocleavable linkers on the $NaYF_4$ UCNPs of the previous system.[23] Since the DMTr group is already present during the SPS of oligonucleotides, its use to quantify loading capacity is highly advantageous compared to other methods, such as utilizing additional fluorescent markers like AlexaFluor 546.[23]

The same assay was performed to quantify the number of PCOs grafted to the nanoparticle surface by click chemistry, using *N*,*N*,*N*′,*N*″,*N*″-pentamethyldiethylenetriamine (PMDETA) as a ligand to protect the DNA. In this case, however, there was concern that the presence of Tris in the oligonucleotide sample would inhibit the copper catalyst, as has been previously reported.[47,48] To overcome this potential issue, a larger excess of $CuSO_4$ was utilized. This route was deemed successful, as an average of 5.3×10^3 PCOs per nanoparticle (29 μmol g^{-1}) was measured from the trityl assay, corresponding to a 41% loading onto the AzSiUCNP surface. Due to the larger size of the PCOs compared to the propargyl nucleoside, it was expected that the loading capacity would be lower in this case. Compared to other reported oligonucleotide/NP values, this value is quite high, with reports of loadings as low as 6 oligonucleotides/nanoparticle (50 nm $NaYF_4$:Yb^{3+}/Tm^{3+} UCNPs)[49] to 75 oligonucleotides/nanoparticle (50 nm silica-coated gold nanoparticles).[50] Unfortunately, many systems ambiguously report the loading values in terms of molar ratios or weight percentages, making a direct comparison difficult.[23,24,51] This demonstrates both the advantage of using highly-efficient click chemistry and covalent conjugation, as electrostatic loading presumably suffers from repulsion between neighbouring oligonucleotide molecules as their numbers increase. A larger number of PCOs per nanoparticle is especially attractive for therapeutic use, as this translates to a smaller number of nanoparticles required to achieve a therapeutic oligonucleotide dose. Furthermore, this fundamental quantitative data is imperative in a therapeutic context, allowing one to accurately determine dosage of oligonucleotide administered to a biological system. To our knowledge, this is the first example of using the DMTr assay to quantify oligonucleotide loading onto a nanoparticle surface.

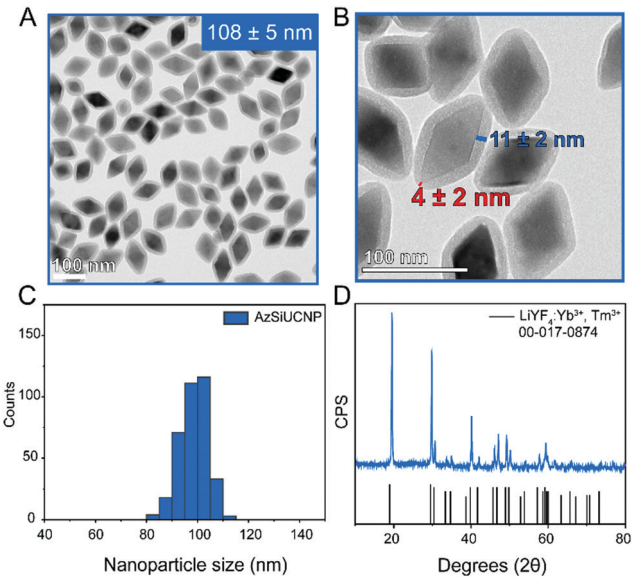

Fig. 2 (A) TEM image of AzSiUCNPs (B) TEM image of the AzSiUCNPs with corresponding silica shell thickness at sides and apex of nanoparticle. (C) Size distribution of AzSiUCNPs. (D) Powder X-ray diffractogram of UCNPs.

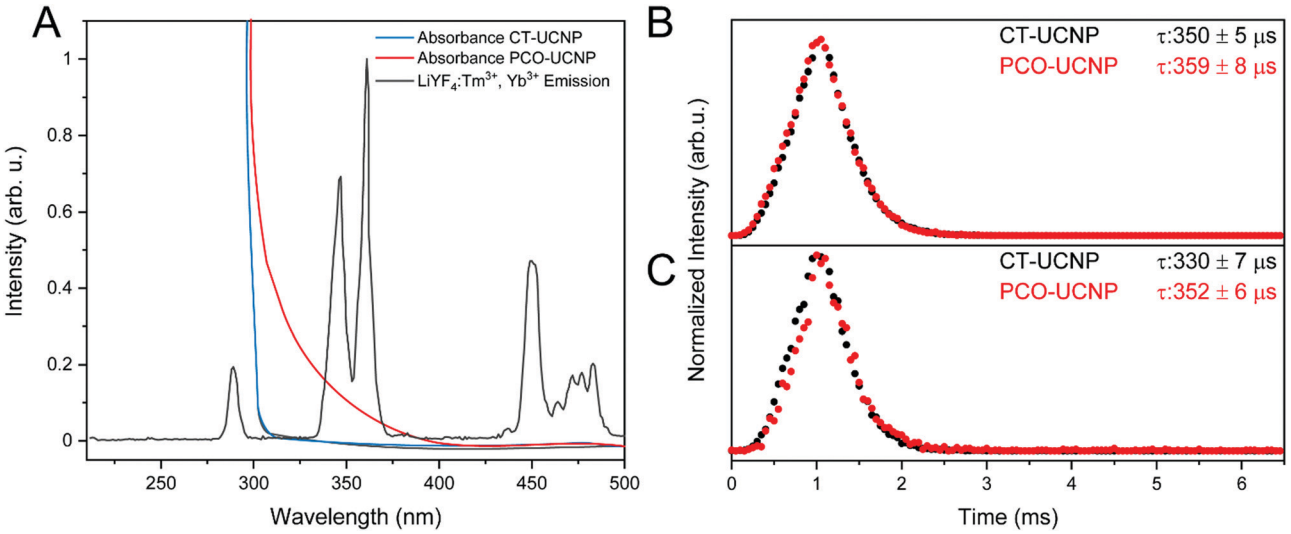

Fig. 3 (A) Upconversion emission spectrum of AzSiUCNPs under 976 nm excitation (1 mg mL^{-1}, black trace), absorbance of control oligonucleotide (blue trace) and photocleavable oligonucleotide (red trace). (B) Lifetimes of CT-UCNP (black) and PCO-UCNP (red) as powders under 976 nm excitation. (C) Lifetimes of CT-UCNP (black) and PCO-UCNP (red) in solution under 976 nm excitation.

Energy transfer studies and luminescence dynamics of Tm^{3+} and the photocleavable oligonucleotide

As shown in Fig. 3A, the control oligonucleotide sequence exhibits overlap with the $^1I_6 \rightarrow {}^3H_6$ transition but not the $^1I_6 \rightarrow {}^3F_4$, $^1D_2 \rightarrow {}^3H_6$ transitions due to the absorption of the oligonucleotide nucleobases. The modified PCO containing an *o*-nitrobenzyl moiety exhibits good spectral overlap with all of the UV emissions of the AzSiUCNPs, which facilitates energy transfer *via* radiative or non-radiative mechanisms. Emission spectroscopy was performed on the control-UCNP (CT-UCNP) and PCO-UCNP samples, with respect to bare AzSiUCNPs, in order to evaluate the energy transfer efficiency in terms of change in the emission intensity in the absence and presence of the photocleavable moiety, respectively (Fig. S9, ESI†). As expected, a decrease in emission intensity is observed for the UV emission bands, but not the blue-emitting bands, due to a lack of spectral overlap in that region. The change in emission intensity in the presence of the PCO corresponds to an energy transfer efficiency of 35%, which could be due to radiative or non-radiative energy transfer processes. The control-UCNPs exhibited a slight decrease in UV intensity, amounting to 3.3% energy transfer, likely due to the overlap with the $^1I_6 \rightarrow {}^3H_6$ transition.

To evaluate the overall dynamics of the upconversion emissions and the mechanism of energy transfer between the oligonucleotide and UCNP, the luminescence lifetimes of the $^1D_2 \rightarrow {}^3H_6$ transition were recorded between the control-UCNP and PCO-UCNP systems, as solid powders (Fig. 3B) and aqueous colloidal suspensions (Fig. 3C). When comparing the control oligonucleotide system as a powder (350 ± 5 μs) or dispersed in water (330 ± 7 μs), the slight shortening of the lifetime can be attributed to the phonon energies of water minimally quenching the luminescence closer to the surface of the nanoparticle. While the average silica thickness exceeds 10 nm, which should properly protect the nanoparticle from environmental influences, there are thinner regions near the apices of the nanoparticle (Fig. 2B).[52,53] These regions are somewhat vulnerable to solvent quenching, which can propagate *via* energy migration to Yb^{3+} ions throughout the lattice.[54] The photocleavable oligonucleotide system follows a similar difference in powder (359 ± 8 μs) and in solution (352 ± 6 μs), though the change in lifetime is much smaller. It is hypothesized that the PCO, with its bulky and hydrophobic 5′-*O*-DMTr group, may be more effective at excluding any residual water from reaching the surface of the nanoparticle, thus minimizing surface quenching even further.

In order to observe any Förster resonance energy transfer (FRET) between the activators in the nanoparticle and the photocleavable oligonucleotide, the lifetime should be shorter with respect to the control system. However, this is not observed, and in fact the lifetime of the photocleavable system is longer than the control in both solution and solid powder, by 6.3% and 2.5%, respectively. This could be caused by small loading differences of the oligonucleotides in the control and photocleavable systems onto the AzSiUCNP surface, presumably from the Tris present in the PCO samples, which could interfere with the CuAAC reaction, as previously discussed. Because the difference in lifetime is of the same magnitude as that of the powder and solution comparisons, it is postulated that vibrational frequencies from the oligonucleotides themselves are the influential factor on the observed lifetimes.

Since these systems are intended for use in aqueous or biological environments, the use of a thick silica shell avoids overwhelming solvent quenching, a phenomenon otherwise known to be a major problem for upconverting nanoparticle luminescence.[55] A consequence of this protection is the lack of FRET between the nanoparticle activators and the oligonucleotide. Thus, the activators in the UCNP emit UV, and the light is subsequently absorbed by the PCO. Essentially, the utilization of a thick silica shell facilitates the promotion of electrons to the UV-emitting excited states of Tm^{3+}, vital for both FRET and

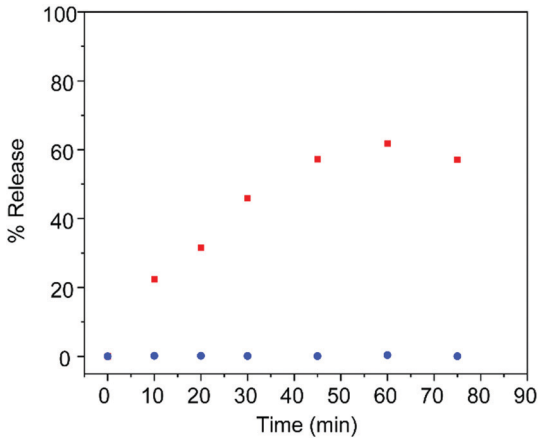

Fig. 4 Percent cleavage of oligonucleotide from PCO-UCNP (red) *versus* the CT-UCNP (blue) under 976 nm excitation in solution at different time points.

radiative energy transfer, but allows only for radiative energy transfer to occur. The two most similar systems do not report luminescence dynamics, but are also expected not to undergo FRET, as they utilize bulky polyelectrolytes or silica shells with thiosuccinimide linkers, both of which result in increased distance between the activators and the photocleavable group.[23,24]

Upconversion-induced photorelease of oligonucleotides

After establishing the mechanism of energy transfer, the photocleavage efficiency of the PCO-UCNP system was evaluated. First, as previously discussed, it is possible to initiate electrostatic interactions between oligonucleotides and cationic surfaces. Thus, zeta potential studies were used to determine the surface charge of the AzSiUCNPs were negative, such that upon photorelease the oligonucleotides would not immediately bind to the surface *via* electrostatic interactions. Indeed, the AzSiUCNPs exhibited a negative surface zeta potential (−20.3 mV, pH = 7), confirming that the oligonucleotides would be repelled from the UCNP surface upon cleavage (Fig. S11A, ESI†). After the PCO was linked to the UCNPs, the zeta potential of the conjugate was −33.3 mV (Fig. S11B, ESI†), confirming the presence of the oligonucleotide's negatively charged phosphodiester backbone.

To evaluate the extent of the photorelease, a colloidal dispersion of the PCO-UCNP system (0.1 mg mL^{-1} in water, pH 7) was irradiated with continuous-wave 976 nm excitation (0.622 W cm^{-2} with a beam area of 0.060 cm^2 at 1/*e* maximum beam intensity[18]) and the solution was evaluated at different time points (Fig. 4). To separate the released oligonucleotides from the PCO-UCNPs, the dispersion was centrifuged to pellet the PCO-UCNPs and the supernatant was evaluated by UV-visible absorption spectroscopy by the absorption of DNA at 260 nm. Based on the calculated loading amounts and the extinction coefficient at 260 nm of the PCO (146 400 L cm^{-1} mol^{-1}), complete release of the PCO in solution would equate to an absorbance of 0.4 at 260 nm. Therefore, the percentage release was determined with respect to the observed absorbance at each time point and the theoretical absorbance maximum. 32% photorelease was realized after just 10 minutes of irradiation, with the release reaching a plateau after one hour of irradiation, at 62% (Fig. 4). As expected, the CT-UCNP system exhibited no photorelease under identical experimental conditions (Fig. 4).

Unfortunately, it is difficult to compare these results to other systems as generally, no percent release is reported. However, this amount of release is similar to one system that utilizes electrostatic interactions to conjugate oligonucleotides to the UCNP surface *via* a polyelectrolyte comb, reporting 60% release at pH 7 after 1 hour of irradiation.[24] It should be noted that the power density used for their study (2.6 W cm^{-2}) was more than double what was used here. Thus, our approach represents a significant improvement in potential applicability, as the maximum permissible skin exposure of 976 nm excitation to humans is 0.713 W cm^{-2} for a beam width of 3.5 mm, for an exposure of up to 8.3 hours.[56]

Since it is well-known that Cu(I) species can cause cleavage of the oligonucleotide strand,[57] the photoreleased products in the supernatant were evaluated. Importantly, no significant strand cleavage was observed in the gel (Fig. S12, ESI†) and the major species was confirmed to be the released 5′-phosphate dT_{18} oligonucleotide by mass spectrometry (Fig. S13, ESI†). Clearly, the Cu(I) stabilizing ligand (PMDETA) utilized in the click reaction was sufficient at protecting the DNA. Additionally, the supernatant of the irradiated CT-UCNP sample was also loaded into the gel, but no oligonucleotide was observed in the lane, demonstrating the necessity of the *o*-nitrobenzyl moiety for proper photorelease.

Conclusions

This platform was developed with versatility, expandability and optimizing target interaction in mind. To this end, it would be compatible with loading single-stranded antisense oligonucleotides (with a uniformly ionic or neutral backbone, or a hybrid of the two), PMOs and siRNA duplexes. The latter type being possible due to the 5′-phosphate group that is present after photorelease, a necessary functionality in the guide strand for proper recognition by the cellular machinery.[58] Moreover, the position of the photocleavable group in the oligonucleotide can be easily altered depending on the nucleotide site chosen for the coupling of the PCP according to the SPS protocol. This system can also be expanded by extending the PCO at the 5′-end (after the alkyne functionality) by SPS, imparting further desirable properties. In fact, there exists a wide variety of commercially available 5′-modifiers, such as the GalNAc phosphoramidite (enabling tissue targeting for therapeutic applications) and dye phosphoramidites (to confer fluorescence for diagnostic applications). Lastly, unlike some conjugates that take advantage of stimuli-responsive oligonucleotide release,[59] the current system releases the oligonucleotide without bulky covalent attachments leftover, even with further 5′-extension, which could lead to sub-optimal binding affinity with target RNA or protein.

In summary, we have generated and characterized a silica-coated $LiYF_4$:Yb^{3+}/Tm^{3+} UCNP–oligonucleotide conjugate,

connected through a stable triazole linkage. The alkyne and photocleavable phosphoramidites at the core of this conjugate were synthesized with an emphasis on both the greenness and practicality of the process. By retaining the 5′-*O*-DMTr group on the PCO after purification, a trityl assay could be performed, determining the loading to be an average of 5.3×10^3 PCOs per nanoparticle. Efficient photorelease upon NIR excitation was demonstrated, where 62% of the oligonucleotides were released after irradiation for 1 hour. The control sequence lacking the photocleavable group showed no photorelease after being exposed to the same conditions. Analysis of the photoproducts by gel electrophoresis and mass spectrometry demonstrated that the undamaged 5′-phosphate dT_{18} oligonucleotide was released. Evaluation of the luminescence lifetimes was used to determine that a radiative energy transfer process was the main mechanism through which energy transfer between the Tm^{3+} emitters in the UCNPs and the photocleavable group occurred. While this is not as favorable as FRET, which is inherently more efficient, the thick silica shell was justified to prevent water quenching that would otherwise have adverse effects on the photorelease efficiency.

By placing the majority of the crucial functional moieties (DMTr, alkyne, *o*-nitrobenzyl) on the oligonucleotide, rather than the linkers growing off the UCNPs, we have simplified and streamlined the generation of this covalent conjugate system, as the oligonucleotides can be generated in an already optimized (phosphoramidite chemistry) and automated fashion (SPS), on a scale that generates appreciable amounts. The simplicity of the trityl assay is evident, as the DMTr group utilized for quantification is already present during oligonucleotide synthesis, whereby no additional group is necessary.

With the foundation of the UCNP–oligonucleotide conjugate system and simplified quantification method in place, efforts will now shift towards studying the *in vitro* photorelease and gene knockdown efficacy of a modified antisense oligonucleotide.

Author contributions

C. L. and G. A. M. gave equal contribution to conceptualization of the project and writing the manuscript. C. L. carried out all synthesis and characterization of small molecules and oligonucleotides, as well as gel electrophoresis. G. A. M. carried out all synthesis and characterization of the upconverting nanoparticles and oligonucleotide–UCNP conjugates, as well as the photocleavage experiments. S. L. M. carried out the lifetime studies and data analysis of the oligonucleotide–UCNP conjugates. K. D. aided in the purification of the oligonucleotides. J. A. C. and C. J. W. supervised the project. All authors contributed to reviewing and editing the manuscript.

Conflicts of interest

There are no conflicts of interest to declare.

Acknowledgements

This research was supported by the Natural Sciences and Engineering Research Council of Canada (NSERC) grants to C. J. W. and J. A. C. J. A. C. is a Concordia University Research Chair in Nanoscience, and is thankful to Concordia University for support. C. L. is thankful for support from NSERC (Alexander Graham Bell Canada Graduate Scholarship - Doctoral - CGS-D) and the Fonds de recherche du Québec – Nature et technologies (Bourse de doctorat). C. L. is also grateful for additional support from the Miriam Aaron Roland Fellowship. G. A. M. would like to thank NSERC for support through the Alexander Graham Bell CGS-D award. S. L. M. would like to thank NSERC for support through the CGS-M award. K. D. is thankful for support from NSERC (Canada Graduate Scholarship - Master's - CGS-M). We thank Dr Anne Noronha for assistance with solid-phase synthesis and Cynthia Messina for helpful discussions.

References

1 M. N. Stojanovic, P. de Prada and D. W. Landry, Aptamer-based folding fluorescent sensor for cocaine, *J. Am. Chem. Soc.*, 2001, **123**, 4928–4931.
2 J. Liu and Y. Lu, Rational Design of 'Turn-On' Allosteric DNAzyme Catalytic Beacons for Aqueous Mercury Ions with Ultrahigh Sensitivity and Selectivity, *Angew. Chem., Int. Ed.*, 2007, **46**, 7587–7590.
3 J. Zhao, J. Gao, W. Xue, Z. Di, H. Xing, Y. Lu and L. Li, Upconversion Luminescence-Activated DNA Nanodevice for ATP Sensing in Living Cells, *J. Am. Chem. Soc.*, 2018, **140**, 578–581.
4 C. Rinaldi and M. J. A. Wood, Antisense oligonucleotides: The next frontier for treatment of neurological disorders, *Nat. Rev. Neurol.*, 2018, **14**, 9–21.
5 A. Fire, S. Xu, M. K. Montgomery, S. A. Kostas, S. E. Driver and C. C. Mello, Potent and specific genetic interference by double-stranded RNA in Caenorhabditis elegans, *Nature*, 1998, **391**, 806–811.
6 J. M. Campbell, T. A. Bacon and E. Wickstrom, Oligodeoxynucleoside phosphorothioate stability in subcellular extracts, culture media, sera and cerebrospinal fluid, *J. Biochem. Biophys. Methods*, 1990, **20**, 259–267.
7 A. M. Iribarren, B. S. Sproat, P. Neuner, I. Sulston, U. Ryder and A. I. Lamond, 2′-*O*-alkyl oligoribonucleotides as antisense probes, *Proc. Natl. Acad. Sci. U. S. A.*, 1990, **87**, 7747–7751.
8 S. K. Singh, P. Nielsen, A. A. Koshkin and J. Wengel, LNA (locked nucleic acids): synthesis and high-affinity nucleic acid recognition, *Chem. Commun.*, 1998, 455–456.
9 Y. Huang, Preclinical and Clinical Advances of GalNAc-Decorated Nucleic Acid Therapeutics, *Mol. Ther.--Nucleic Acids*, 2017, **6**, 116–132.
10 T. Lehto, K. Ezzat, M. J. A. Wood and S. El Andaloussi, Peptides for nucleic acid delivery, *Adv. Drug Delivery Rev.*, 2016, **106**, 172–182.

11 D. B. Rozema, D. L. Lewis, D. H. Wakefield, S. C. Wong, J. J. Klein, P. L. Roesch, S. L. Bertin, T. W. Reppen, Q. Chu, A. V. Blokhin, J. E. Hagstrom and J. A. Wolff, Dynamic PolyConjugates for targeted in vivo delivery of siRNA to hepatocytes, *Proc. Natl. Acad. Sci. U. S. A.*, 2007, **104**, 12982–12987.

12 D. Zheng, D. A. Giljohann, D. L. Chen, M. D. Massich, X. Q. Wang, H. Iordanov, C. A. Mirkin and A. S. Paller, Topical delivery of siRNA-based spherical nucleic acid nanoparticle conjugates for gene regulation, *Proc. Natl. Acad. Sci. U. S. A.*, 2012, **109**, 11975–11980.

13 Y. Y. C. Tam, S. Chen and P. R. Cullis, Advances in lipid nanoparticles for siRNA delivery, *Pharmaceutics*, 2013, **5**, 498–507.

14 C. H. Kapadia, J. R. Melamed and E. S. Day, Spherical Nucleic Acid Nanoparticles: Therapeutic Potential, *BioDrugs*, 2018, **32**, 297–309.

15 M. K. G. Jayakumar, N. M. Idris and Y. Zhang, Remote activation of biomolecules in deep tissues using near-infrared-to-UV upconversion nanotransducers, *Proc. Natl. Acad. Sci. U. S. A.*, 2012, **109**, 8483–8488.

16 R. Naccache, Q. Yu and J. A. Capobianco, The Fluoride host: Nucleation, growth, and upconversion of lanthanide-doped nanoparticles, *Adv. Opt. Mater.*, 2015, **3**, 482–509.

17 S. L. Maurizio, G. Tessitore, G. A. Mandl and J. A. Capobianco, Luminescence dynamics and enhancement of the UV and visible emissions of Tm3+ in LiYF4:Yb3+,Tm3+ upconverting nanoparticles, *Nanoscale Adv.*, 2019, **1**, 4492–4500.

18 P. A. Rojas-Gutierrez, S. Bhuckory, C. Mingoes, N. Hildebrandt, C. DeWolf and J. A. Capobianco, A Route to Triggered Delivery via Photocontrol of Lipid Bilayer Properties Using Lanthanide Upconversion Nanoparticles, *ACS Appl. Nano Mater.*, 2018, **1**, 5345–5354.

19 G. A. Mandl, P. A. Rojas-Gutierrez and J. A. Capobianco, A NIR-responsive azobenzene-based supramolecular hydrogel using upconverting nanoparticles, *Chem. Commun.*, 2018, **54**, 5847–5850.

20 W. Shen, J. Zheng, Z. Zhou and D. Zhang, Approaches for the synthesis of o-nitrobenzyl and coumarin linkers for use in photocleavable biomaterials and bioconjugates and their biomedical applications, *Acta Biomater.*, 2020, **115**, 75–91.

21 M. M. Rubner, D. E. Achatz, H. S. Mader, J. A. Stolwijk, J. Wegener, G. S. Harms, O. S. Wolfbeis and H. A. Wagenknecht, DNA 'Nanolamps': 'Clicked' DNA conjugates with photon upconverting nanoparticles as highly emissive biomaterial, *ChemPlusChem*, 2012, **77**, 129–134.

22 L.-L. Li, P. Wu, K. Hwang and Y. Lu, An exceptionally simple strategy for DNA-functionalized Up-conversion nanoparticles as biocompatible agents for nanoassembly, DNA delivery, and imaging, *J. Am. Chem. Soc.*, 2013, **135**, 2411–2414.

23 Y. Yang, F. Liu, X. Liu and B. Xing, NIR light controlled photorelease of siRNA and its targeted intracellular delivery based on upconversion nanoparticles, *Nanoscale*, 2013, **5**, 231–238.

24 H. Zhao, W. Hu, H. Ma, R. Jiang, Y. Tang, Y. Ji, X. Lu, B. Hou, W. Deng, W. Huang and Q. Fan, Photo-Induced Charge-Variable Conjugated Polyelectrolyte Brushes Encapsulating Upconversion Nanoparticles for Promoted siRNA Release and Collaborative Photodynamic Therapy under NIR Light Irradiation, *Adv. Funct. Mater.*, 2017, **27**, 1–14.

25 A. N. Bashkatov, E. A. Genina, V. I. Kochubey and V. V. Tuchin, Optical properties of human skin, subcutaneous and mucous tissues in the wavelength range from 400 to 2000 nm, *J. Phys. D: Appl. Phys.*, 2005, **38**, 2543–2555.

26 S. Wu and H. J. Butt, Near-Infrared-Sensitive Materials Based on Upconverting Nanoparticles, *Adv. Mater.*, 2016, **28**, 1208–1226.

27 S. C. Alley, D. R. Benjamin, S. C. Jeffrey, N. M. Okeley, D. L. Meyer, R. J. Sanderson and P. D. Senter, Contribution of linker stability to the activities of anticancer immunoconjugates, *Bioconjugate Chem.*, 2008, **19**, 759–765.

28 C. P. Ryan, M. E. B. Smith, F. F. Schumacher, D. Grohmann, D. Papaioannou, G. Waksman, F. Werner, J. R. Baker and S. Caddick, Tunable reagents for multi-functional bioconjugation: Reversible or permanent chemical modification of proteins and peptides by control of maleimide hydrolysis, *Chem. Commun.*, 2011, **47**, 5452–5454.

29 A. D. Baldwin and K. L. Kiick, Tunable degradation of maleimide-Thiol adducts in reducing environments, *Bioconjugate Chem.*, 2011, **22**, 1946–1953.

30 K. Zheng, Y. Chen, J. Wang, L. Zheng, M. Hutchinson, J. Persson and J. Ji, Characterization of Ring-Opening Reaction of Succinimide Linkers in ADCs, *J. Pharm. Sci.*, 2019, **108**, 133–141.

31 B. Q. Shen, K. Xu, L. Liu, H. Raab, S. Bhakta, M. Kenrick, K. L. Parsons-Reponte, J. Tien, S. F. Yu, E. Mai, D. Li, J. Tibbitts, J. Baudys, O. M. Saad, S. J. Scales, P. J. McDonald, P. E. Hass, C. Eigenbrot, T. Nguyen, W. A. Solis, R. N. Fuji, K. M. Flagella, D. Patel, S. D. Spencer, L. A. Khawli, A. Ebens, W. L. Wong, R. Vandlen, S. Kaur, M. X. Sliwkowski, R. H. Scheller, P. Polakis and J. R. Junutula, Conjugation site modulates the in vivo stability and therapeutic activity of antibody-drug conjugates, *Nat. Biotechnol.*, 2012, **30**, 184–189.

32 K. Nienhaus and G. U. Nienhaus, Protein corona around nanoparticles—recent advances and persisting challenges, *Curr. Opin. Biomed. Eng.*, 2019, **10**, 11–22.

33 P. S. Miller, Oligonucleoside methylphosphonates as antisense reagents, *Nat. Bio/Technol.*, 1991, **9**, 358–362.

34 C. J. Wilds, G. Minasov, F. Natt, P. Von Matt, K. H. Altmann and M. Egli, Studies of a chemically modified oligodeoxynucleotide containing a 5-atom amide backbone which exhibits improved binding to RNA, *Nucleosides, Nucleotides Nucleic Acids*, 2001, **20**, 991–994.

35 J. Summerton and D. Weller, Morpholino Antisense Oligomers: Design, Preparation, and Properties, *Antisense Nucleic Acid Drug Dev.*, 1997, **7**, 187–195.

36 T. C. Roberts, R. Langer and M. J. A. Wood, Advances in oligonucleotide drug delivery, *Nat. Rev. Drug Discovery*, 2020, **19**, 673–694.

37 S. Cirak, V. Arechavala-Gomeza, M. Guglieri, L. Feng, S. Torelli, K. Anthony, S. Abbs, M. E. Garralda, J. Bourke, D. J. Wells, G. Dickson, M. J. Wood, S. D. Wilton, V. Straub, R. Kole, S. B. Shrewsbury, C. Sewry, J. E. Morgan, K. Bushby and F. Muntoni, Exon skipping and dystrophin restoration in patients with Duchenne muscular dystrophy after systemic phosphorodiamidate morpholino oligomer treatment: An open-label, phase 2, dose-escalation study, *Lancet*, 2011, **378**, 595–605.

38 C. W. Tornøe, C. Christensen and M. Meldal, Peptidotriazoles on solid phase: [1,2,3]-Triazoles by regiospecific copper(i)-catalyzed 1,3-dipolar cycloadditions of terminal alkynes to azides, *J. Org. Chem.*, 2002, **67**, 3057–3064.

39 V. V. Rostovtsev, L. G. Green, V. V. Fokin and K. B. Sharpless, A stepwise Huisgen cycloaddition process: Copper(i)-catalyzed regioselective 'ligation' of azides and terminal alkynes, *Angew. Chem., Int. Ed.*, 2002, **41**, 2596–2599.

40 P. T. Anastas and J. C. Warner, *Green Chemistry: Theory and Practice*, Oxford University Press, New York, 1998, p. 30.

41 H. C. Brown and O. J. Cope, Hydroboration. XXIII. Directive Effects in the Hydroboration of Representative Allyl Derivatives. The Elimination Reaction of β-Substituted Organoboranes, *J. Am. Chem. Soc.*, 1964, **86**, 1801–1807.

42 J. S. Davies, C. L. Higginbotham, E. J. Tremeer, C. Brown and R. C. Treadgold, Protection of hydroxy groups by silylation: Use in peptide synthesis and as lipophilicity modifiers for peptides, *J. Chem. Soc., Perkin Trans. 1*, 1992, 3043–3048.

43 H. C. Brown and J. C. Chen, Hydroboration. 57. Hydroboration with 9-Borabicyclo[3.3.1]nonane of Alkenes Containing Representative Functional Groups, *J. Org. Chem.*, 1981, **46**, 3978–3988.

44 P. Ordoukhanian and J. S. Taylor, Design and Synthesis of a Versatile Photocleavable DNA Building Block. Application to Phototriggered Hybridization, *J. Am. Chem. Soc.*, 1995, **117**, 9570–9571.

45 M. J. Damha, P. A. Giannaris and S. V. Zabarylo, An improved procedure for derivatization of controlled-pore glass beads for solid-phase oligonucleotide synthesis, *Nucleic Acids Res.*, 1990, **18**, 3813–3821.

46 R. P. Iyer, J. E. Coughlin and S. Padmanabhan, Rapid functionalization and loading of solid supports, *Org. Prep. Proced. Int.*, 2005, **37**, 205–212.

47 V. Hong, S. I. Presolski, C. Ma and M. G. Finn, Analysis and optimization of copper-catalyzed azide-alkyne cycloaddition for bioconjugation, *Angew. Chem., Int. Ed.*, 2009, **48**, 9879–9883.

48 Y. Yang, X. Yang and S. H. L. Verhelst, Comparative analysis of click chemistry mediated activity-based protein profiling in cell lysates, *Molecules*, 2013, **18**, 12599–12608.

49 M. Kumar and P. Zhang, Highly sensitive and selective label-free optical detection of DNA hybridization based on photon upconverting nanoparticles, *Langmuir*, 2009, **25**, 6024–6027.

50 K. L. Young, A. W. Scott, L. Hao, S. E. Mirkin, G. Liu and C. A. Mirkin, Hollow spherical nucleic acids for intracellular gene regulation based upon biocompatible silica shells, *Nano Lett.*, 2012, **12**, 3867–3871.

51 S. Jiang and Y. Zhang, Upconversion nanoparticle-based FRET system for study of siRNA in live cells, *Langmuir*, 2010, **26**, 6689–6694.

52 D. J. Gargas, E. M. Chan, A. D. Ostrowski, S. Aloni, M. V. P. Altoe, E. S. Barnard, B. Sanii, J. J. Urban, D. J. Milliron, B. E. Cohen and P. J. Schuck, Engineering bright sub-10-nm upconverting nanocrystals for single-molecule imaging, *Nat. Nanotechnol.*, 2014, **9**, 300–305.

53 M. I. Saleh, B. Rühle, S. Wang, J. Radnik, Y. You and U. Resch-Genger, Assessing the protective effects of different surface coatings on NaYF4:Yb3+,Er3+ upconverting nanoparticles in buffer and DMEM, *Sci. Rep.*, 2020, **10**, 1–11.

54 S. Fischer, N. D. Bronstein, J. K. Swabeck, E. M. Chan and A. P. Alivisatos, Precise Tuning of Surface Quenching for Luminescence Enhancement in Core–Shell Lanthanide-Doped Nanocrystals, *Nano Lett.*, 2016, **16**, 7241–7247.

55 R. Arppe, I. Hyppänen, N. Perälä, R. Peltomaa, M. Kaiser, C. Würth, S. Christ, U. Resch-Genger, M. Schäferling and T. Soukka, Quenching of the upconversion luminescence of NaYF4:Yb3 +,Er3+ and NaYF4:Yb3+,Tm3+ nanophosphors by water: The role of the sensitizer Yb3+ in non-radiative relaxation, *Nanoscale*, 2015, **7**, 11746–11757.

56 American National Standard for Safe Use of Lasers (ANSI Z136.1-2014), Laser Institute of America, Orlando, 2014, p. 68.

57 C. J. Burrows and J. G. Muller, Oxidative nucleobase modifications leading to strand scission, *Chem. Rev.*, 1998, **98**, 1109–1151.

58 F. Frank, N. Sonenberg and B. Nagar, Structural basis for 5′-nucleotide base-specific recognition of guide RNA by human AGO2, *Nature*, 2010, **465**, 818–822.

59 L. Shi, W. Wu, Y. Duan, L. Xu, Y. Xu, L. Hou, X. Meng, X. Zhu and B. Liu, Light-Induced Self-Escape of Spherical Nucleic Acid from Endo/Lysosome for Efficient Non-Cationic Gene Delivery, *Angew. Chem., Int. Ed.*, 2020, **59**, 19168–19174.